

Instationary heat and mass transfer phenomena in additive manufactured open cell polyhedral structures for automotive catalysis



V. Papetti^{a,*}, P. Dimopoulos Eggenschwiler^a, A. Della Torre^b, G. Montenegro^b, A. Onorati^b, A. Ortona^c, G. Koltsakis^d

^aAutomotive Powertrains Technologies Laboratory, Empa, Swiss Federal Laboratories for Materials Testing and Research, Dübendorf, Switzerland

^bDipartimento di Energia, Politecnico di Milano, Milano, Italy

^cSUPSI, Switzerland

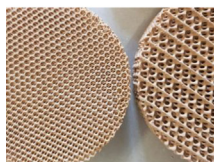
^dAristotle University Thessaloniki, Greece

HIGHLIGHTS

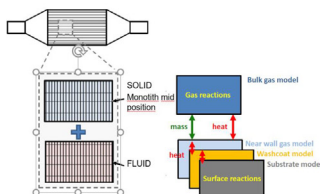
- Warm up during cold starts inside an open cell catalytic converter is analyzed.
- CFD simulations of the transient heat and mass transfer launched in OpenFOAM.
- Open cell polyhedral lattices have higher mass and heat transfer than honeycombs.
- Optimal converter design for faster warm up.
- Dimensionless model of the thermal response of the open cell catalytic converter.

GRAPHICAL ABSTRACT

Additive Manufactured Open cell



CFD Simulations



T_F = Fluid Temperature

$T_0 = T_{S0} = T_S(t = 0s)$

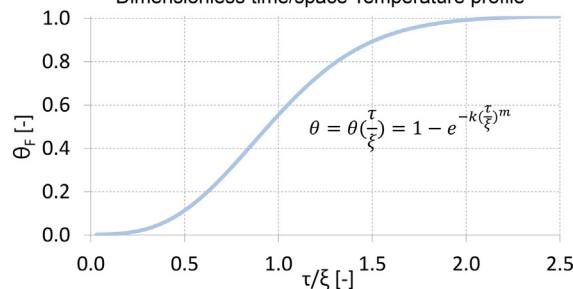
$T_{F,in}$ = Inlet Fluid Temperature

(x, t) = Coordinates

$$\frac{\tau}{\xi} = \frac{\dot{m}_F c_{PF}}{A_{S,FRONT} \rho_S c_S} \frac{t}{x}$$

$$\theta_F = \frac{T_F - T_0}{T_{F,in} - T_0}$$

Dimensionless time/space Temperature profile



ARTICLE INFO

Article history:

Received 21 July 2020

Received in revised form 18 November 2020

Accepted 9 January 2021

Available online 18 January 2021

Keywords:

Automotive catalysts open cell polyhedral lattices

Additive manufacturing

Cold starts

Heat and mass transfer in catalysts

Catalyst numerical simulations

Dimensionless approach

ABSTRACT

Additive Manufactured (AM) Open Cell Polyhedral lattices are novel substrates for automotive catalytic converters due to promising properties. The present investigation focuses on heat and mass transfer with chemical reactions during cold starts, based on numerical simulations in OpenFOAM and dimensionless analytical analysis. The numerical model consists of a multi-region approach with overlapping meshes for fluid and solid regions, in order to simulate the presence of porous substrates. Experimental results from first vehicle-size AM catalysts are used as a basis. The catalyst heat-up is characterized by two distinguished phases: the initial phase where heat is convected from the inflowing gases to the catalyst and the following phase which is governed by the heat released by the chemical reactions. The impact of different operating parameters, lattice and converter geometries has been quantified. The introduction of dimensionless temperature, time and space, evidences the similarity of the initial warm-up phase.

© 2021 Elsevier Ltd. All rights reserved.

* Corresponding author at: Überlandstrasse 129, Dübendorf 8600, Zürich ZH (CH), Switzerland.

E-mail address: viola.papetti@empa.ch (V. Papetti).

Nomenclature

$A_{S,FRONT}$	Frontal Area	q_{react}	Heat released due to reactions per unit of converter volume
$A_{//}$	Lateral Area	Re	Reynolds number based on strut diameter
AM	Additive Manufacturing	S_V	specific surface
C_{PF}	Fluid isobaric specific heat capacity	S_W	Wetted surface
C_S	Solid specific heat capacity	Sc	Schmidt number
C45	AM catalyst substrate consisting of cubes as elementary cells rotated by 45° so that one spatial diagonal of the cube is aligned to the main gas flow	Sh	Sherwood number
D_{CO}	Diffusion coefficient related to CO species in the fluid	t	Dimensioned time coordinate
d_F	Fluid characteristic dimension	T_{Fin}	Inlet fluid temperature
d_S	Strut diameter	T_F	Fluid temperature
h	Heat transfer coefficient	T_S	Solid, thus catalytic converter, temperature
HC:	Honeycomb catalyst substrate (conventional)	T_{SO}	Initial solid temperature
K_{CO}	Mass transfer coefficient related to CO species in the fluid	T_0	Reference temperature, reference temperature in dimensionless definitions
L	Catalytic Converter length	μ_∞	Upstream velocity
L_C	Cell length	V	Volume of entire catalyst
L_S	Strut length (in case of Cubic elementary cells $L_C = L_S$)	v_{in}	Mean gas velocity upstream the catalyst entrance
LHV	Lower Heating Value	x	Dimensioned space coordinate
\dot{m}_F	Fluid mass flowrate	X_{COF}	Fluid molar concentration of CO
\dot{m}_{rCO}	Reacting CO mass flowrate	X_{COS}	Molar concentration of CO on solid (converter) surface
$\dot{m}_{v,rCO}$	Reacting CO mass flowrate per unit of converter volume	X_{COin}	Fluid inlet molar concentration of CO
m_S	Solid mass flowrate	ε	Solid porosity
MM_F	Fluid molar mass	η_{CO}	CO Conversion through the catalyst
MM_{CO}	CO molar mass	θ	Dimensionless temperature difference
Nu	Nusselt number	θ_S	Dimensionless Solid temperature
NTU_θ	number of transfer units	θ_F	Dimensionless Fluid temperature
\dot{q}	Heat flux from the fluid to the solid per unit of converter volume	Λ	Dimensionless solid conductivity
\dot{Q}	Heat flux from the fluid to the solid	λ_F	Fluid thermal conductivity
q	Heat from the fluid to the solid per unit of converter volume	λ_S	Solid thermal conductivity
Q	Heat released due to reactions	ξ	Dimensionless space coordinate
q_{conv}	Convected heat from the fluid to the solid per unit of converter volume	ξ_i	Dimensionless space coordinate for species i
		ξ/τ	dimensionless time–space coordinate
		Π_p	Permeability dimensionless number
		ρ_S	Solid density
		τ	Dimensionless time coordinate

1. Introduction

Currently, light duty vehicles (LDV) with spark-ignition engines and Three-Way-Catalysts (TWCs) reach almost 100% pollutant conversion during normal high temperature operating conditions. This is not the case during cold starts and warming up phases. During cold starts, a catalytic converter at low temperature is suddenly exposed to exhaust gas of moderate temperature, thus chemical reactions, if any, are very slow. Newest targeted measurements and simulations performed in our laboratory on a Euro 6 gasoline vehicle have shown that 20% of the CO, 96% of the unburned hydrocarbons (THCs) and 65% of the NOx during the WLTC cycle are emitted in the first 300 s following the engine cold start (at 20 °C). Moreover, all newest engine concepts, oriented towards reduction of the specific fuel consumption, have lower exhaust gas temperatures, leading to new challenges in the management of the after-treatment system, in particular during cold starts. Hybrid powertrains increase the related difficulties based on the intermittent combustion engine operations. Under these premises, several measures are under evaluation for shortening the cold start catalyst inactivity period: decrease of engine efficiency in order to increase exhaust gas enthalpy, electrical preheating of the gas, or microwave heating of the catalyst (Papetti and Dimopoulos Eggenschwiler, 2019).

Innovative design of open-cell catalytic substrates represents a promising alternative to the benchmark of honeycombs (HC). Open-cell catalytic substrates are a network of solid struts creating tortuous paths that enhance gas-wall interactions and contribute to lower thermal inertia (Lucci et al., 2017). The result is higher conversion efficiencies (Busse et al., 2018; Giani et al., 2005; Pangarkar et al., 2008; Bracconi et al., 2018), an improve of the global heat transfer performances, lower cold start emissions and higher flow uniformity, a key factor for catalyst durability (Gaiser et al., 2003; Zygourakis, 1989; von Rickenbach et al., 2015; Dimopoulos Eggenschwiler et al., 2009; Della Torre et al., 2015; Dimopoulos Eggenschwiler et al., 2018). They also allow more flexibility in the geometrical configuration of the reactor (Koltsakis et al., 2008). Lucci et al. (2017) has shown that regular open cell polyhedral structures outperform with respect to the equivalent foam (at the same porosity ε and strut diameter d_s). Lu et al. (1998) proposed a cubic cell model that was used to analyze mass transfer and pressure drop data. Giani et al. (2005) showed that a regular cubic-module structure is particularly beneficial in applications where external (fluid–solid) heat and mass transport are relevant. The same authors have conducted a geometrical optimization of the unit cell: they have identified in the rotated cubic cell the structure with the highest tradeoff between conversion and pressure loss (Papetti et al., 2018). Busse et al. (2018)

focuses on the potential heat transfer intensification of a new generation of periodic open cellular structures cellular structures. Only recently, such regular structures have been realized in cordierite by additive Manufacturing in real vehicle dimensions (Papetti et al., 2018; Dimopoulos Eggenschwiler et al., 2018; Santoliquido et al., 2017). Overall, the structures realized showed thicker struts and lower reacting surface. The produced catalysts, according to the authors, the worldwide first AM automotive catalysts, have been tested on a vehicle chassis dynamometer. Apart from cold starts, where performances, in particular for CO oxidation, were lower than expected, testing revealed promising characteristics with only 1/5 of the precious metals.

The transient heat and mass transfer characteristics of catalysts are of major importance in order to minimize the heat-up time. (Depcik and Assanis, 2005) offers an exhaustive overview of one-dimensional automotive catalyst modeling. Heck et al. (1976) showed that a simpler one-dimensional model is adequate for predicting catalyst behavior. Young and Finlayson (1974) developed a two-dimensional channel model for a honeycomb using orthogonal collocation focusing on the applicability of the quasistatic assumption for the gas phase for transient cases. Numerous models have specifically focused on the complex transient phenomena during cold starts. Oh et al. (1980), Oh and Cavendish (1985) and Oh and Cavendish (1985) use a model for the pellet type catalyst for the prediction and parametric analysis of vehicle exhaust emissions during the warm-up. The same authors studied the response of a honeycomb converter to step changes in feedstream temperature using a one-dimensional adiabatic channel model under laminar flow conditions (Papetti et al., 2019). Lin and Kuo (1988) has numerically investigated the effects of conduction heat transfer in the wall resulting from a step change in uniform wall heat flux. They recognized the ratio of fluid to solid thermal capacities as the more important parameter of the phenomenon. Olek et al. (1991) studied further the case of a fixed wall temperature using a non-standard method of separation of variables. Yan et al. (1989) investigated the role of radial heat conduction in thick-walled pipes, neglecting the axial solid conduction. More complex are models for the three way catalysts, involving oxygen storage and ceria reactions. Koltsakis et al. (1997) modelled the transient behavior of a monolithic TWC (Three Way Catalyst) including the oxygen storage submodel able to account for the redox and temperature dependence of the oxygen availability. They showed that bulk kinetic expressions are sufficient for the prediction of emissions over random driving scenarios, including cold-start phase and legislated driving cycles. Chen et al. (1988) developed a transient three-dimensional model to simulate the thermal and conversion characteristics of nonadiabatic axisymmetric ceramic monolithic converters operating under flow maldistribution conditions. The predicted temperature profiles provide a basis for the analysis of thermal stresses and fatigue in the monolith converter assembly. Several works have also focused on modeling heat and mass transfer mechanisms in open cell structures. Della Torre et al. (2018) used a combination of micro-CT, image-based modeling and CFD to investigate the transient phenomena occurring at the micro-scale level in two different porous substrates: open-cell foams and unstructured filtering media. Previous work of the authors of the present paper, (Lucci et al., 2017), proposed a complete 3D CFD model of a foam based catalytic converter and discussed the effects of varying inflow velocity, inflow CO mass fraction and washcoat surface area (Pt loading). Kopanidis et al. (2010), Krishnan et al. (2006), Bianchi et al. (2012), Bianchi et al. (2013) described the heat transfer in foam based catalytic reactors, Lucci et al. (2014) focused on the mass transfer mechanism. Both mass transfer (chemical reactions) and heat transfer are considered simultaneously, restricted to steady state reactor operation in (von Rickenbach et al., 2015; Gräf et al., 2014). Transient studies

of foam based catalytic reactors are limited to one-dimensional volume averaged models in (Tsinoglou et al., 2009; Tsinoglou et al., 2009).

A small number of works proposed a dimensionless analysis of the heat and mass transfer phenomena inside catalytic converters. Votruba et al. (1975) modelled the heat up mechanism inside a catalytic converter as the thermal response of an adiabatic, thin walled duct subjected to a developing incompressible laminar flow and offered a dimensionless solution of the system of coupled, nonlinear ordinary differential equations. Koltsakis (1997) used a dimensionless approach to examine the temperature evolution of the monolith reactor after a step change of the feed gas inlet temperature. However, up to now, the investigations have been under limited steady state conditions and considering temperature behavior only at inlet and outlet positions. In (Papetti and Dimopoulos Eggenschwiler, 2019) the same authors apply the dimensionless approach to the warm up of a honeycomb substrate and investigate the effects of varying thermophysical boundary conditions.

The present work aims to analyze the fundamental of the cold start characteristics of AM catalysts.

Therefore the standard case was setup where exhaust gases of moderate temperature, typical for the first engine cycles after cold start, flow through, AM catalysts of low initial temperature (typical for a winter day). In order to compare different cases, the exhaust gas flow was kept constant in each case. Specific emphasis was placed in the investigation of the effects of different geometrical dimensions of the AM catalyst, in order to assess the influence of the differences among the realized and simulation derived optimal dimensions. The temperature and flow parameter ranges have been deliberately chosen in order to represent conditions of typical automotive cold starts. Emphasis was given in parameter combinations leading to moderate chemical reactions, avoiding parameters that either result in no reactions or in too fast reactions, in order to achieve a spatial and temporal resolution allowing detailed study of the phenomena. The approach combines numerical simulations in the environment of OpenFOAM and an analytical dimensionless model for investigating the behavior of the catalytic converter along its entire length. The CFD framework is based on a multi-region approach where overlapping meshes, describing fluid and solid regions, are employed in order to model the presence of porous substrates. Specific models are implemented in order to couple fluid and solid regions in terms of heat-transfer and mass-transfer. Catalytic CO oxidation surface reactions are considered. The model is validated with own results (Della Torre et al., 2018).

2. Methodology

2.1. Realization of AM catalytic converters with real vehicle dimensions

Polyhedral open cell converters have been Additive Manufactured by stereolithography. The resulting structures have been obtained in cordierite through the replica method. Subsequently catalytic washcoating followed. Details concerning fabrication, microstructural and mechanical properties of the samples can be found in (Papetti et al., 2018). The results in geometrical properties are reported in Table 1. A graphical representation is also offered in Figs. 1 and 2.

2.2. AM catalysts geometrical characteristics for simulations

The investigations involved geometries with expected improved characteristics as predicted in (Papetti et al., 2018),

Table 1
Geometrical properties of the AM structures realized.

Unitary cell	ε [-]	d_s [mm]	L_c [mm]	S_v [m ² /m ³]
C45	0.82	1.32	4.39	500

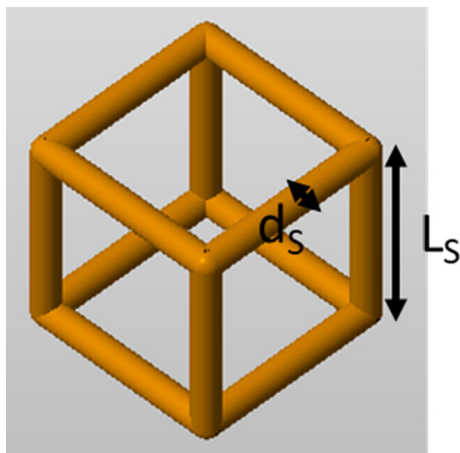


Fig. 1. Unit cell (C45) with basic dimensions.

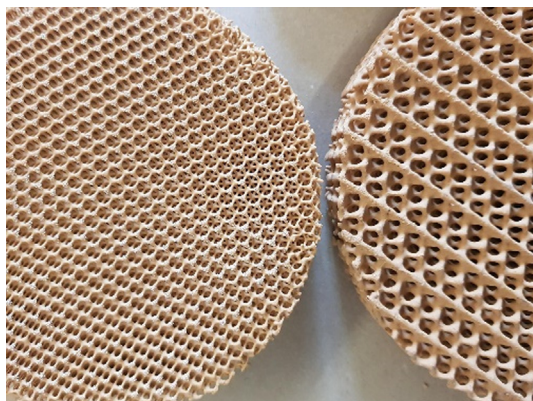


Fig. 2. AM vehicle catalysts with different geometrical properties.

which can still be considered realistic, given manufacturing constraints of current stereolithography developments.

The unitary cell is cubic rotated 45° so that one spatial diagonal of the cube is aligned to the main gas flow. This elementary cell is called C45. This is the optimal configuration as identified in (Papetti et al., 2018). Three specific geometries are here considered, denoted by AM1, AM2 and AM3. Their main geometrical properties are described in Table 1. The converter material remains cordierite.

2.3. Experiments on the chassis dynamometer

The AM described in Table 1 has been tested on a vehicle on a chassis dynamometer on several driving cycles.

During the driving cycles, the exhaust gas temperature and pressure have been measured upstream and downstream of the catalyst. Upstream the catalyst an exhaust probe was mounted and connected via a 5-m long heated pipe to the exhaust gas analyzer Horiba MEXA 9200DF. Tailpipe emissions have been conducted through a second 5-m heated pipe to a second Horiba MEXA 9200DF. The carbon monoxide (CO), carbon dioxide (CO₂), oxygen (O₂), nitrogen oxide (NO_x), and hydrocarbon (THC) concen-

trations were measured at 10 Hz sampling rate. It is assumed that the NO_x concentration measured corresponds entirely to nitric oxide (NO), and that the HC concentration measured corresponds entirely to C₃H₆. The ambient temperature was around 20 °C.

2.4. Simulation model

The different additive manufactured catalyst geometries described in Table 2 are simulated in OpenFOAM. CO oxidation is taken into account under oxygen abundance, i.e., typical Diesel Oxidation Catalyst conditions. The CFD model adopts a multi-region approach, distinguishing two regions, the fluid and the coated substrate (catalytic converter region), thus the fundamental equations for the fluid and the catalytic converter regions are solved on different meshes. The two grids are overlapping where both gas phase and solid phase coexist, for example in the catalyst porous regions, while in the pipe/cone regions only the fluid mesh is defined. The volume occupied by each phase is defined by a volumetric fraction coefficient computed as the ratio between the volume occupied by the corresponding phase and the total volume. The coupling between the two regions is managed between own sub-models, which describe the mass and heat transfer between fluid and catalyst regions. On the solid region, the species and energy conservation equations are solved; on the fluid region, the set of governing equations of conservation of mass, momentum, energy and species is closed with the perfect gas equation of state. The thermal properties of the multi-component mixture are determined on the basis of the JANAF tables. A Sutherland model is applied for the computation of the transport properties, in order to take into account the temperature dependence of viscosity. The mass diffusivity is modelled under the assumption of Schmidt number equal to 1 in order to reduce the computational burden. The chemistry is modelled with Langmuir-Hinshelwood-type expression in which the reaction rate parameters have been previously tuned with experiments. The permeability model that defines the fluid-dynamic resistance encountered by the fluid flowing through the porous medium depends on the geometrical properties of the substrate and the instantaneous fluid dynamics conditions. It is determined on the basis of Reynolds number (Re) with correlations in the form $\Pi_p = F(\text{Re}, d_f)$ by results of own numerical simulations at the micro scales. Specific correlations of Nu and Sh in function of Re are exploited to specify the transfer of heat/mass on the basis of the actual fluid-dynamic conditions and the properties of the fluid/solid. Even in this case, the correlations in the form of $\text{Nu} = F(\text{Re}, \text{Pr}, d_f)$ and $\text{Sh} = F(\text{Re}, \text{Sc}, d_f)$ are results of previous simulations performed by the present authors. The catalyst is treated as a generic porous medium characterized by some general parameters: porosity ε , the specific surface S_v , the characteristic size of the pores/channels open to the fluid d_f (in the three directions, if the media is anisotropic), the characteristic size of the solid structure/walls of the substrate d_s , the washcoat thickness d_w . These parameters are then exploited in the other submodels to calculate the actual fluid dynamics and heat/mass transfer properties based on suitable correlations for the specific medium.

The model has been validated in previous works of the present authors by simulating a honeycomb TWC converter (Della Torre et al., 2018). Simulation results related to a WLTC cycle have been compared with corresponding experiments in house in terms of CO, NO_x and THC cumulative emissions. Differences between the

Table 2
Geometrical properties of the AM structures simulated.

	Unitary cell	ε [-]	d_s [mm]	L_c [mm]	S_v [m ² /m ³]
AM1	C45	0.8	0.8	2.08	896
AM2	C45	0.9	0.5	3.43	733
AM3	C45	0.85	0.5	2	1050

cases of an AM polyhedral openfoam converter with respect to an HC geometry are related to the fluid characteristics correlations specified (Nu, Sh, pressure loss). It can be thus deduced that the model is valid also for AM converters.

2.5. Analytical model equations and assumptions

An analytical approach is proposed, on the one hand, for identifying possible simplifications, and, on the other hand, for highlighting basic dependencies useful for interpreting the simulation results. Here we consider the flow through the AM structure as an internal flow with irregular boundaries, given the tortuosity of the struts. Heat transfer to ambient compared to the convective heat transfer in the channels is of minor importance (Della Torre et al., 2018), especially during the warm-up phase studied here, where the temperature difference between converter and ambient are low, thus we treat the converter as adiabatic. The struts are considered as very thin, so that no radial solid-phase temperature gradients are expected. For the heat transfer cases met in catalytic reactors, the wall heat capacity is large compared with the heat capacity of the fluid. Thus, during a small-time increment, only the effect of varying wall temperature needs to be taken into account and the fluid heat capacity effect can be ignored (Koltsakis, 1997). The assumption of quasi-steady state heat transfer has been widely used in literature (Oh et al., 1980; Yan et al., 1989; Bianchi et al., 2012). Radiation effects are not included, since they are not significant in the case of low temperatures (Hayes and Kolaczowski, 1994). Moreover, in accordance with (Kays and Crawford, 1993), in the mass flow range considered, axial gas conduction effects are excluded. The flow velocity range considered corresponds to a Mach number considerably smaller than 0.2, so the flow can be considered incompressible. Assuming quasi-steady state, incompressible flow, considering an infinitesimal volume of the fluid phase, in the case when chemical reactions have not a significant contribution, the solid energy balance during the transient can be formulated as:

$$\frac{\partial T_S}{\partial t} = \frac{\lambda_S}{\rho_S c_S} \frac{\partial^2 T_S}{\partial x^2} + \frac{\dot{m}_F C_{PF}}{A_{S,FRONT} \rho_S c_S} \frac{\partial T_F}{\partial x} \quad (1)$$

The corresponding fluid energy balance as:

$$\frac{\partial T_F}{\partial x} = - \frac{4Nu\lambda_F}{\dot{m}_F C_{PF}} (T_F - T_S) \quad (2)$$

While the species balance as:

$$u_\infty \frac{dX_{CO,F}}{dx} = \dot{n}_{CO} S_v = K_{CO} (X_{CO,F} - X_{CO,S}) = \frac{ShD_{CO}}{d_F} (X_{CO,F} - X_{CO,S}) \quad (3)$$

From which, following relation can be derived:

$$\frac{dX_{CO,F}}{dx} = \frac{ShD_{CO}}{d_F u_\infty} (X_{CO,F} - X_{CO,S}) \quad (4)$$

Due to the spatial geometrical characteristics of very large length compared to characteristic strut diameter, the flow and thermal boundary layers are fully developed over the largest part of the reactor. In the present study, heat transfer augmentation

due to flow entrance effects will not be considered and the hypothesis of constant Nu number for the entire channel will be used (von Rickenbach et al., 2015; Lucci et al., 2014; von Rickenbach et al., 2015; Koltsakis, 1997).

The convective heat flux per unit volume exchanged can be obtained according to the following balance equation:

$$\dot{q}_{conv,it} = \frac{\dot{m}_F C_{PF}}{\Delta V} (T_{F,it} - T_{F,i+1,t}) \quad (5)$$

Diffusion limitations in the pores of the washcoat are not accounted. The fundamental assumption of quasi-steady state has been used: the rate of molecular diffusion from the fluid to the solid walls is equal to the rate of chemical reactions for each species (CO) on the solid, implying that there is no species accumulation on the solid catalytic surface. Considering this assumption, the mass balance equation in the gas phase gives the expression:

$$X_{CO,F,i+1} = X_{CO,S,i} + (X_{CO,F,i} - X_{CO,F,i+1}) \quad (6)$$

This assumption is realistic for steady-state operation, but not necessarily for operation under transient temperature and composition conditions. In our model, the quasi-steady approach expressed by Eq. (6) is retained, aiming at keeping model complexity, and thus flexibility, to acceptable levels. Thus, the total mass flux of the specie in question (CO) transferred from the fluid to the solid, being equal to the mass reacting on the wall, can be obtained by:

$$\dot{m}_{rCO,i} = \frac{\dot{m}_F M_{CO}}{MM_F \Delta V} (X_{CO,F,i} - X_{CO,F,i+1}) \quad (7)$$

2.6. Dimensionless quantities and approximation possibilities

In Eqs. (1) and (2) a dimensionless temperature difference can be introduced for the fluid and for the solid, leading to Eqs. (8) and (9) (Koltsakis, 1997). Please notice that T_F and T_S are function of time and space, thus also θ_F and θ_S :

$$\theta_F = \frac{T_F - T_0}{T_{F,in} - T_0} \quad (8)$$

$$\theta_S = \frac{T_S - T_0}{T_{F,in} - T_0} \quad (9)$$

The reference temperature was chosen as the initial solid temperature $T_0 = T_S(t = 0) = T_{S0}$. Dimensionless fluid temperature θ_F represents the ratio between the instantaneous solid–fluid temperature difference to the initial solid–fluid temperature difference. Under the hypothesis of negligible reactions, which is true in the first period of the warm-up, dimensionless solid temperature represents the increment of solid temperature difference with respect to the maximum increment it can reach. A dimensionless length, ξ , was introduced as:

$$\xi = \frac{4Nu\lambda_F x}{\dot{m}_F C_{PF}} \quad (10)$$

Moreover, a dimensionless time was introduced:

$$\tau = \frac{4Nu\lambda_F t}{A_{S,FRONT} \rho_S C_S} \quad (11)$$

Similarly a dimensionless conductivity Λ can be introduced:

$$\Lambda = \frac{4Nu\lambda_F A_{S,FRONT} \lambda_S}{\dot{m}_F^2 C_{PF}^2} \quad (12)$$

Using Eqs. (8)–(12) simplifies Eqs. (1) and (2), to:

$$\frac{\partial \theta_F}{\partial \tau} = \theta_S - \theta_F \quad (13)$$

$$\frac{\partial \theta_S}{\partial \tau} = \Lambda \frac{\partial^2 \theta_S}{\partial \zeta^2} - \frac{\partial \theta_F}{\partial \zeta} \quad (14)$$

3. Results and discussion

The typical automotive catalyst cold start is characterized by gases arriving in the entrance of the catalytic converter (coming from the engine) at moderate temperatures. In order to analyze and compare the fundamental mechanisms involved, the cases in this study have been setup based on the following pattern: exhaust gas of constant temperature T_{Fin} and mass flow rate \dot{m}_F flowing in a catalytic converter (volume of 2lt) with an initial, lower and uniform temperature T_{S0} . The temporal and spatial evolution of temperatures and concentrations, as well as of further characteristic properties of the heat and mass transfer are the main focus. The results presented and discussed in the following sections show the detailed temporal evolution. Should dependencies on further parameters be the focus, typical time instants have been selected. For assessing the spatial distribution, the observed quantities are displayed at the entrance ($x = 0$), three equidistant points inside the converter, ($x = 1/4L = 0.038$ m), ($x = 1/2L = 0.076$ m), ($x = 3/4L = 0.1148$ m), and at the exit ($x = L = 0.1524$ m) of the converter. Apart from the influence of different (additive manufactured) catalyst geometries, the present study analyses in detail the influence of different T_{Fin} , T_{S0} and \dot{m}_F . The values chosen for these parameters are typical for automotive cold starts, but also such that the phenomena in focus are neither too fast nor too slow.

3.1. Measured cold start emissions

Fig. 3 shows measured conversion efficiencies of the AM catalyst (the geometrical details are reported in Table 1) on the chassis dynamometer over the WLTC in terms of CO, THC and NOx.

There are two aspects that are common among all the three species: lower conversions are detected at low and at high velocity ranges. Deficiencies at higher velocity is due to mass transfer limitations. This was the focus of the work of the same authors published in (Papetti et al., 2018), where optimal converter

characteristics for maximum chemical conversion are derived. The present paper focuses on the low velocity range, which is typical of cold starts related phenomena. The same optimization intention is presented here: a deep analysis of the cold starts phenomena and of the geometrical effects is offered for deriving optimal converter design.

3.2. Basic characteristics of the cold start behavior of the AM1 catalytic converter

Fig. 4 presents TF and TS time histories at the different local positions inside the AM1, as described in Table 2. The results correspond to the case of $T_{Fin} = 425$ K, $T_{S0} = 260$ K and $\dot{m}_F = 0.0172$ kg/s. Dashed lines represent TF, while solid lines TS (catalytic converter).

At the entrance of the converter, the fluid is instantly cooled down to a temperature of 410 K, while the solid is instantly warmed up to a temperature of 310 K, both temperatures according to the thermal effusivities involved. In the entrance region thereafter, the fluid and solid heat up, until the fluid reassumes its inflowing temperature T_{Fin} and, shortly after, TS reaches TF ($t \sim 15$ s). In more downstream positions, the fluid is cooled down towards $T_{S0} = 260$ K. So, for the first seconds, $T_F(x = 1/4L) = T_{S0}$ and, in a similar manner, for $t < 10$ s $T_F(x = 1/2L) = T_{S0}$ as well as for $t < 20$ s $T_F(x = 3/4L) = T_{S0}$ and for $t < 25$ s $T_F(x = L) = T_{S0}$. In all locations, TF and TS increase in time towards the temperature of the entering gases.

Based on these observations and on all the cases examined, the catalyst warm-up can be divided in two different phases. The initial phase with heat transferred from the fluid to the solid (convection) until $T_S = T_F = T_{Fin}$. In this phase, temperature in downstream locations are lower than in the upstream (at the same t). Following this, the second phase starts as soon as $T_F > T_S$ (not clearly discernible in Fig. 4a, but clear in the magnification enclosed in Fig. 4b). Here the heat-up is primarily based on the heat released by the chemical reactions in the solid (which in turn is convected back to the fluid). Certainly, first, weak chemical reactions have initiated earlier, (as can be seen in Figs. 5 and 6). Indeed, first oxidation reactions occur in the very first part of the catalytic converter as soon as $T_S \geq 373$ K. It is also in the first quarter that $T_S > T_F > T_{Fin}$ occurs, exemplarily for $x = 1/4L$ at $t \rightarrow 30$ s. The heat produced by the chemical reactions is transferred to the fluid (convection) as well as conducted inside the solid (as long as solid downstream parts have lower temperatures). A local equilibrium is reached almost instantly, exhibiting stationary temperatures at each location. The heat generated is taken up by the fluid and contributes to the heat up of the downstream catalyst sections, which, in turn, leads to locally higher reaction rates. Thus, the local temperatures increase in the downstream, in contrast to the first phase. The very small increase of the temperature in the last quarter is due to the

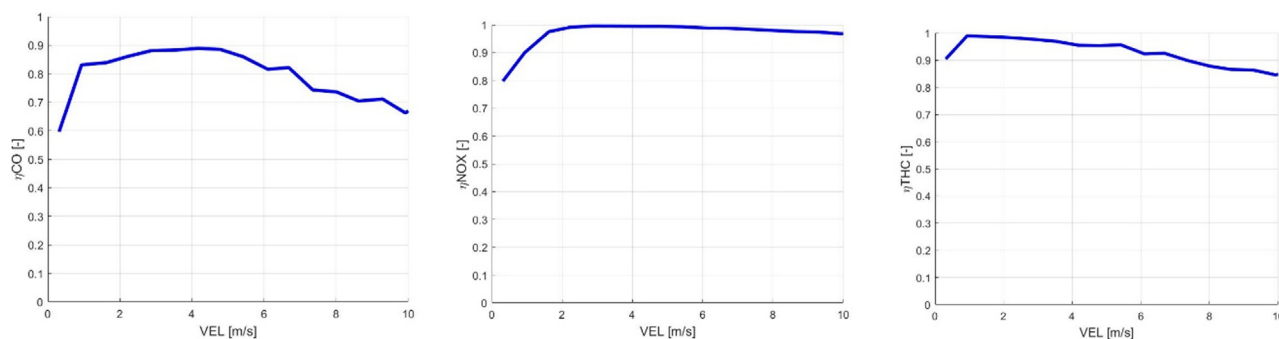


Fig. 3. Experimental conversion efficiencies in terms of CO, NOx and THC during the WLTC for an Additive Manufactured converter (geometrical properties reported in Table 1). Measurements are performed on the chassis dynamometer of Empa with a EURO6 Gasoline Engine.

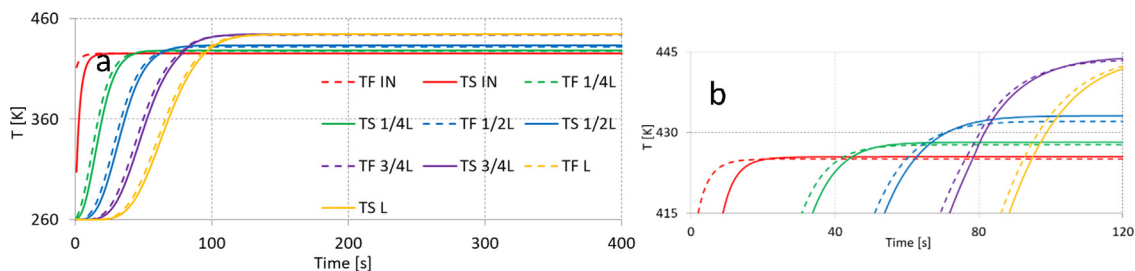


Fig. 4. Fluid, TF, (dashed lines) and solid, TS, (solid lines) temperature time histories in the selected locations inside AM1 ($T_{Fin} = 425$ K, $T_{S0} = 260$ K and $\dot{m}_F = 0.0172$ kg/s). (b) is a detail of (a).

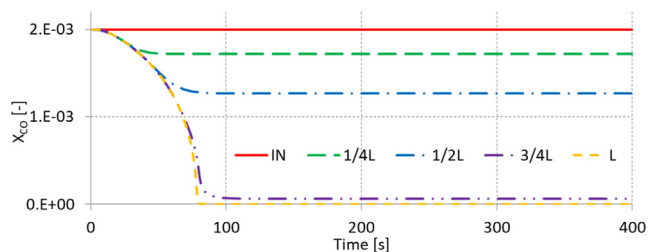


Fig. 5. CO molar concentration, X_{CO} , time histories in the selected locations inside the catalytic converter ($T_{Fin} = 425$ K, $T_{S0} = 260$ K and $\dot{m}_F = 0.0172$ kg/s).

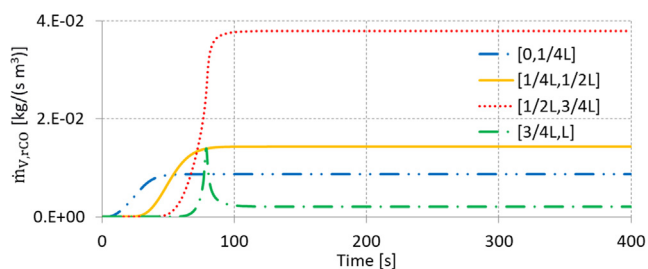


Fig. 6. Reacting CO mass rates, $\dot{m}_{V,rCO}$, in the different converter quarters ($T_{Fin} = 425$ K, $T_{S0} = 260$ K and $\dot{m}_F = 0.0172$ kg/s).

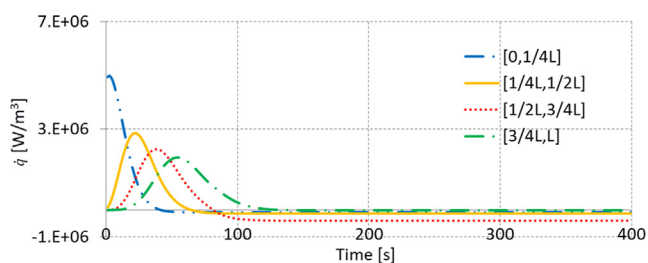


Fig. 7. Heat exchanged from the fluid to the solid, \dot{q} , integrated over the different converter quarters ($T_{Fin} = 425$ K and $\dot{m}_F = 0.0172$ kg/s, $T_{S0} = 260$ K).

low amount of remaining CO, as almost the entire CO is oxidized in the upstream catalyst parts (more details in Fig. 7).

Fig. 5, which shows the time history of X_{CO} , provides additional evidence for the above discussion. The same case of Fig. 4 at $T_{S0} = 260$ K, $T_{Fin} = 425$ K and $\dot{m}_F = 0.0172$ kg/s is considered. The dependence of X_{CO} from the evolving (increasing) T_S is evident. First reaction traces can be discerned slightly before 10 s at the catalytic converter entrance, when T_S reaches circa 373 K. X_{CO} at the exit of the first quarter of the catalytic converter starts decreasing, falling below the $X_{CO,in}$. For $t < 30$ s the X_{CO} in the remaining catalyst parts is identical with the X_{CO} in the first quarter, evidencing that no reactions happen in the downstream yet (consistent with

the low temperature at these locations). At about $t = 42$ s it is achieved a local equilibrium between the heat released by the chemical reactions and the heat convected to the gases. The temperature in the first quarter of the converter stabilizes (see Fig. 4) and the corresponding reaction rate of CO oxidation stabilizes as well, thus, consequently, X_{CO} at $x = 1/4L$ remains constant over time (also clearly seen in Fig. 6). Additional decrease of X_{CO} in the next quarter of the catalytic converter evidences the onset of the reactions there. Here the reaction rate is slightly higher due to the slightly higher temperature, a consequence of both the convection heat transfer and exothermic heat released by the reactions happening in the first quarter. In the same manner, around 50 s, the entire first half of the catalytic converter reaches equilibrium and first reactions are evident in the third quarter. After $t = 69$ s, reactions start also in the last quarter of the catalytic converter. CO conversion is complete soon after. Almost the entire reactions happen in the first three quarters of the catalytic converter length. The steady state temperature increases along the catalytic converter up to 444 K in the last quarter (see also related discussion with Eqs. (15)–(17)).

The discussed phenomena are confirmed when taking into account $\dot{m}_{F,V,rCO}$ in each of the catalyst quarters under consideration (see Fig. 6). For $t < 7$ s no reactions are evident. Thereafter initial reactions start at the entrance of the first quarter and equilibrium is reached at around $t = 42$ s. Reactions in the second quarter start later, stabilizing at a slightly higher reaction rate. The reaction rate in the third quarter is the highest, while the remaining CO in the last quarter is very low, leading to lowest $\dot{m}_{F,rCO}$ there. In the last quarter, only a peak is evidenced at $t = 75$ s. At this time, the reactions in the third quarter have not reached the highest rate yet, thus allowing some more CO slip to the last quarter. After $\dot{m}_{F,rCO}$ in the third quarter stabilizes at a high value ($3.8 \cdot 10^{-2}$ kg/(sm^3)), only a low amount of CO reaches the fourth quarter and reacts there.

These observations are also reflected in \dot{q} from the fluid to the solid, as shown in Fig. 7. In order from upstream to downstream, each catalyst quarter experiences the initial heat-up phase, where the solid is heated up by the gases (positive \dot{q}). As soon as the first phase is completed, first chemical reactions start and the heat flow reverses (negative) from the solid to the fluid. For the initial temperature differences chosen here, the convective heat flux in the initial warm-up phase, as shown in Fig. 7, is significantly larger in respect to the heat released by the chemical reactions in the second phase. The peak of the heat flux in the initial warm-up phase is highest in the catalytic converter entrance and declines in the downstream. This is explained taking into account the temporal and local evolution of the temperatures (Fig. 4); the temperature gradients decline with time and space (downstream). The declining temperature gradients, however, result in (temporal) slower heat up. Thus, the duration of the initial heat-up phase increases in the downstream parts. Table 3 summarizes the duration of the initial heat up phase as well as the energy exchanged in this phase.

Table 3

Duration and value of heat exchanged during the initial heat-up phase (from fluid to solid) in comparison to the heat released by the chemical reactions in the second phase (assuming identical duration of both phases). The energy released by the chemical reactions in the last quarter is not reported because of the very small amount of CO left from the preceding quarters, allowing no direct comparison.

Catalyst part	Duration of the initial phase, heat from fluid to solid [s]	Heat exchanged (initial phase from fluid to solid) q [kJ/m ³]	Heat released by the chemical reactions in the second phase q [kJ/m ³]
[0,1/4L]	41	$8 \cdot 10^4$	$3.17 \cdot 10^3$
[1/4L, 1/2L]	64	$8.48 \cdot 10^4$	$8.33 \cdot 10^3$
[1/2L, 3/4L]	85	$8.51 \cdot 10^4$	$3.04 \cdot 10^4$
[3/4L, L]	130	$9.25 \cdot 10^4$	

\dot{q} in the first phase is almost evenly distributed in the four parts of the catalytic converter under consideration. The subsequent energy released by the chemical reactions (convected back to the fluid and a smaller part conducted within the solid) is also shown in Table 3. For obtaining comparable values of energy in the two phases, for each quarter, the time span used in the second phase is equal to the one characteristic of the first one.

3.3. Influence of the inlet fluid and initial solid temperatures

Fig. 8 compares T_F time histories at $x = 1/2L$ and $x = L$ for $\dot{m}_F = 0.00172$ kg/s for two different T_{Fin} and T_{S0} , thus four different cases, with the case shown in Fig. 4 ($T_{Fin} = 425$ K, and $T_{S0} = 260$ K) as a reference. The initial warm up phase is similar for the four cases. First of all, the duration of the heat-up is very similar for all four cases and seems to be almost independent from the initial temperature differences. In all the cases examined, not only the ones shown in Fig. 8, (with same $\dot{m}_F = 0.00172$ kg/s), some 60 s are needed for the flow to reassume T_{Fin} (410 K and 425 K). After the 60 s, the influence of first chemical reactions is evidenced, heating-up the solid, which in turn heats up the gas (the onset of chemical reactions can be better discerned when examining the reacting mass as in Fig. 8). The equilibrium phase is reached soon thereafter. The different initial temperature gradients however lead to different initial heat-up rates and to different chemical reactions rates, thus also to final equilibrium temperatures. Precisely, the equilibrium phase is almost independent from T_{S0} : cases with the same T_{S0} reach almost the same final temperature, slightly higher than T_{S0} .

These observations are also reflected in \dot{q} time history. The values related to the second catalyst quarter [1/4L, 1/2L] are shown in Fig. 9. The process however is similar for all the quarters. Each catalyst quarter has first to be heated up by the gases (positive heat values). As soon as the first phase is completed, first chemical reactions start and the heat flow reverses (negative) from the solid to the fluid. In more detail, the peak of the heat flux in the initial

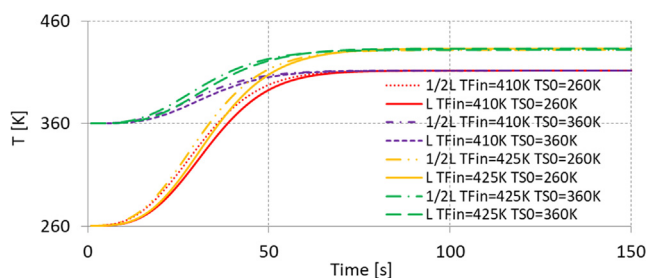


Fig. 8. T_F time histories inside AM1 (at 1/2L and at L), for different $T_{Fin} = [410,425]$ K, and $T_{S0} = [260,360]$ K. ($\dot{m}_F = 0.00172$ kg/s).

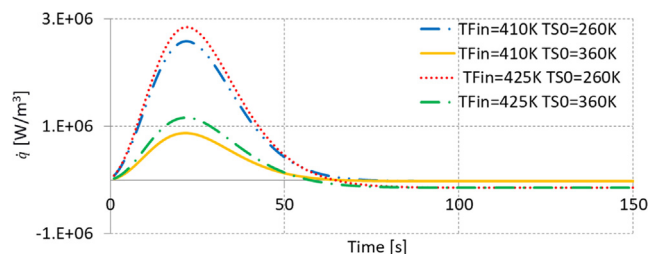


Fig. 9. \dot{q} from the fluid to the solid, integrated in the second quarter ([1/4L,1/2L]), for different $T_{Fin} = [410,425]$ K, and different $T_{S0} = [260,360]$ K ($\dot{m}_F = 0.0172$ kg/s).

warm-up phase (from fluid to solid) is contemporaneous among the cases considered. Different initial temperature gradients lead however to different heat transfer magnitudes: it is highest in the case with higher initial gas–solid temperature difference ΔT ($T_{Fin} = 425$ K and $T_{S0} = 260$ K), and decreases coherently with decreasing ΔT . The subsequent energy released by the chemical reactions is higher in the cases with the higher $T_{Fin} = 425$ K, while it is very small in the cases with $T_{Fin} = 410$ K.

The introduction of the dimensionless temperature difference, θ_F , according to Eq. (8), and dimensionless time, τ , according to Eq. (10), transforms Fig. 8 in Fig. 10. The different combinations of T_{Fin} and T_{S0} , considered both at $x = 1/2L$ and at $x = L$, have similar behavior. As long as no reactions take place, the effects of T_{Fin} and T_{S0} are compensated and the dimensionless time histories overlap at each location along the catalytic converter. As already described in in Par. 3.2, the warm up is faster at $x = 1/2L$ than at $x = L$. These characteristics are evident graphically in Fig. 10 by the fact that the warm up curve is steeper at $x = 1/2L$ than at $x = L$. Considering all the curves corresponding to the same position, substantial deviation of single lines, evidences the onset of the chemical reactions. Earliest oxidation reactions correspond to the case with the highest $T_{S0} = 360$ K.

A more detailed look at the reaction rates in Fig. 11 confirms the above observations. For the two cases with the higher temperature of the solid ($T_{S0} = 360$ K) first reactions are evidenced at around $t = 20$ s, while for the cases with the lower solid temperature some 10 s later. For the further evolution of the reaction rate though, the temperature of the inflowing fluid is decisive. Higher inflowing fluid temperature leads to higher temperature in the equilibrium phase (so after $t > 80$ s for the $T_{Fin} = 425$ K).

Fig. 12 compares the cases of Fig. 8 in terms of X_{CO} at $x = L$ (exit) of the catalytic converter. Concentrations at the exit start to decrease after some 10 s. This is due to initial reactions in the first part of the catalytic converter. This decrease continues steeply in the two cases with high T_{Fin} , less steep in the cases with the lower T_{Fin} . In the former cases, full CO oxidation is reached, sooner for the case with the higher T_{S0} , later in the standard case ($T_{Fin} = 425$ K, and $T_{S0} = 260$ K of Fig. 4). In the latter cases, the reaction rates

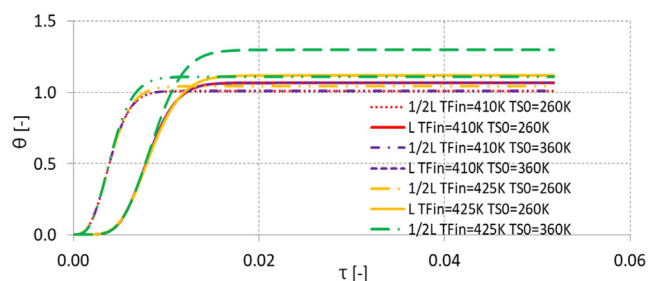


Fig. 10. Dimensionless temperature difference, θ_s , in function of dimensionless time, τ , inside AM1 (at 1/2L and at L), for different $T_{Fin} = [410,425]$ K, and $T_{S0} = [260,360]$ K. ($\dot{m}_F = 0.00172$ kg/s).

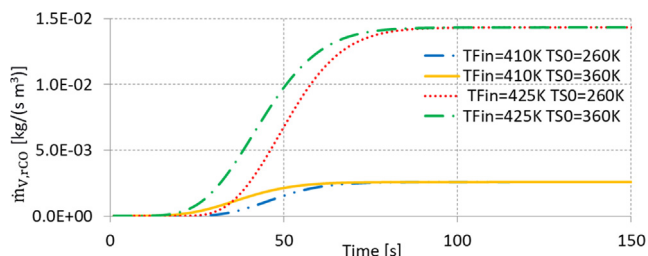


Fig. 11. Reacting CO mass rates, $\dot{m}_{v,CO}$ time history in the second quarter of the catalytic converter ([1/4L,1/2L]), for different $T_{Fin} = [410,425]K$, and different $T_{So} = [260,360]K$, ($\dot{m}_F = 0.0172$ kg/s).

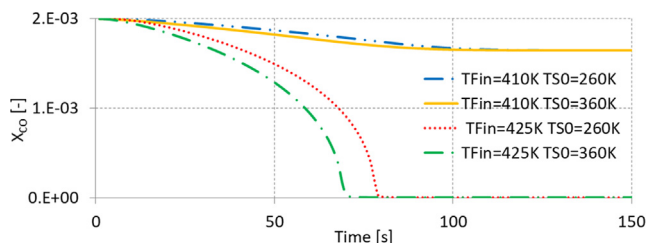


Fig. 12. X_{CO} time histories inside AM1 (at $x = L$), for different $T_{Fin} = [410,425]K$, and different $T_{So} = [260,360]K$ ($\dot{m}_F = 0.0172$ kg/s).

are lower. The differences of the compared time histories are reflected in the cumulative emissions of the compared cases over the entire cold start (not shown here).

3.4. Influence of the fluid mass flow

Fig. 13 shows the influence of varying \dot{m}_F on T_F (Fig. 13 a, b), on $\dot{m}_{v,CO}$ (Fig. 13 c, d), on \dot{q} (Fig. 13 e, f), and on X_{CO} (Fig. 13 g, h). The fluid enters the converter at $T_{Fin} = 425$ K while the solid is at $T_{So} = 260$ K. The results are considered at the time instants of 50 s (Fig. 13 a,c,e,g), and of 400 s (Fig. 13 b,d,f,h). The instant at 400 s shows instead everywhere the second, stationary phase, where equilibrium between the heat released at the solid surface is balanced by the heat transferred to the fluid in all locations. $X_{CO,in}$ is kept constant. Thus, for increasing \dot{m}_F , $\dot{m}_{CO,in}$ increases proportionally.

In Fig. 13a, T_F at $t = 50$ s is described. The behavior of T_S is very similar (to T_F), as discussed in Fig. 4. It is clear that, increasing \dot{m}_F accelerates the heat transfer process. In this sense, the time of $t = 50$ s corresponds to a different progress state of the heat-up process for each \dot{m}_F . For the lowest $\dot{m}_F (=0.0086$ kg/s), the fluid at $x = 1/4L$ has a temperature of around 410 K, while in the downstream parts of the converter it has been cooled down towards the initial T_{So} . With increasing \dot{m}_F , temperatures at the first quarter reach already $T_{Fin} = 425$ K, while those further downstream start to increase. As long as the warm-up is in the initial phase, i.e. $T_S < T_F < T_{Fin}$, increasing \dot{m}_F results in higher temperatures in each of the locations shown; for example at $x = 1/2L$ (and for $t = 50$ s), $T_F(\dot{m}_F = 0.0086$ kg/s) $<$ $T_F(\dot{m}_F = 0.012$ kg/s) $<$ $T_F(\dot{m}_F = 0.02$ kg/s). As already discussed at Figs. 4 and 8, in this initial phase, temperatures in the catalytic converter are higher in the upstream than in the downstream (for a constant \dot{m}_F). The green line indicates the T_{Fin} level, which corresponds to the equilibrium temperature without chemical reactions. Interestingly, at the highest mass flow investigated, $\dot{m}_F=0.036$ kg/s, 50 s are just enough for almost the entire catalytic converter to reach T_{Fin} .

The characteristics in each location change as soon as the second phase is reached ($T_S > T_{Fin}$). Any further condition change has to rely on the heat released by the chemical reactions. The local

reaction rate is dependent on the local temperature (according to the implemented Langmuir Hinshelwood and Arrhenius) as well as on the CO mass transferred from the fluid to the walls, $\dot{m}_{r,CO}$. This is linearly dependent on \dot{m}_F as well as on the local axial concentration gradient. The latter, in turn, is decreasing with $\dot{m}_F^{-0.7}$ (according to Eq. (3)) and considering that for the AM structures in question $Sh \sim \dot{m}_F^{0.3}$ (as reported in (Papetti et al., 2018)). Thus, the mass transferred to the walls increases only with $\dot{m}_F^{0.3}$, and also the heat released by the reaction increases similarly with $\dot{m}_F^{0.3}$. This heat is convected to the fluid; the thermal capacity of the fluid increases linearly with \dot{m}_F . Thus the resulting fluid temperature increase (over T_{Fin}) decreases with increasing \dot{m}_F . This decline is only very small in Fig. 13a (and only for $X = 1/4L$ and $1/2L$) but clear in Fig. 13b for all locations.

Fig. 13c describes $\dot{m}_{v,CO}$ in each converter quarter in function of \dot{m}_F . At the lowest $\dot{m}_F = 0.0086$ kg/s, CO is reacting only in the first quarter. With increasing \dot{m}_F , the reacting CO mass in the first and in the second quarter, first increase and then start slightly decreasing. The increase is due to the increasing temperature during the initial heat up phase. After the completion of the first phase, $\dot{m}_{v,CO}$ decreases based on the slightly decreasing temperature (as discussed for Fig. 13a). Similar phenomena are also encountered in the last two quarters, only later in time.

The two different phases related to the converter warm up mechanism are clearly distinguishable in Fig. 13e, representing \dot{q} between the fluid and the solid in function of \dot{m}_F at $t = 50$ s. According to Eq. (5), \dot{q} is directly proportional to \dot{m}_F and to the fluid axial temperature difference. Positive values correspond to heat transferred from the fluid to the solid, while negative values vice versa. For the lowest $\dot{m}_F = 0.0086$ kg/s, \dot{q} in the first quarter is low, given that at $t = 50$ s the initial heat up phase is almost completed (in the first quarter only). The \dot{q} in the second and third quarter are higher, given that heating up, at $t = 50$ s, here has just started and thus higher temperature gradients prevail. For $\dot{m}_F = 0.0124$ kg/s the initial heat up phase in the first quarter is completed, while the rest of the converter is in the first phase. At higher \dot{m}_F , the first and even the second quarter are in the second phase, as can be seen by the negative heat values. At $t = 50$ s the highest heat is exchanged in the last quarter, where the temperature difference between the solid and the fluid are higher in respect to the other quarters.

The influence of varying \dot{m}_F on X_{CO} at $t = 50$ s is described in Fig. 13g. X_{CO} at the inlet of the converter is indicated in green. As initial reactions occur in the very first part of the catalytic converter (first to be warmed-up), X_{CO} at the end of the first quarter is lower than in the entrance, at $t = 50$ s, already for the lowest \dot{m}_F investigated. Since no reactions occur in the downstream, CO concentrations in the following three quarters are identical, all points coincide (for $\dot{m}_F = 0.0086$ kg/s). For $\dot{m}_F > 0.023$ kg/s reactions occur also in the last downstream quarter of the converter since the concentration there is lower than in the upstream. The behavior in all four quarters of the converter is very similar; with increasing gas mass flow, the CO concentrations at the end of each quarter, first decrease and then increase. The decrease of the concentration is straightforward, associated to the warm up of the catalytic converter and the increasing reaction rates. The following increase of the concentration is explained considering the stagnation and even slight decrease of the reacting mass (see Fig. 13c) during the second catalyst warm up phase, while the inflowing CO mass increases linearly with the gas mass flow, \dot{m}_F .

At $t = 400$ s the converter has reached steady state (no temperature change in time at any location) and it is in the second phase of the heat up in all locations shown in Fig. 13b. Thus, the main driver is the heat released by the chemical reactions on the solid surface and its convection to the fluid, $T_S > T_F$.

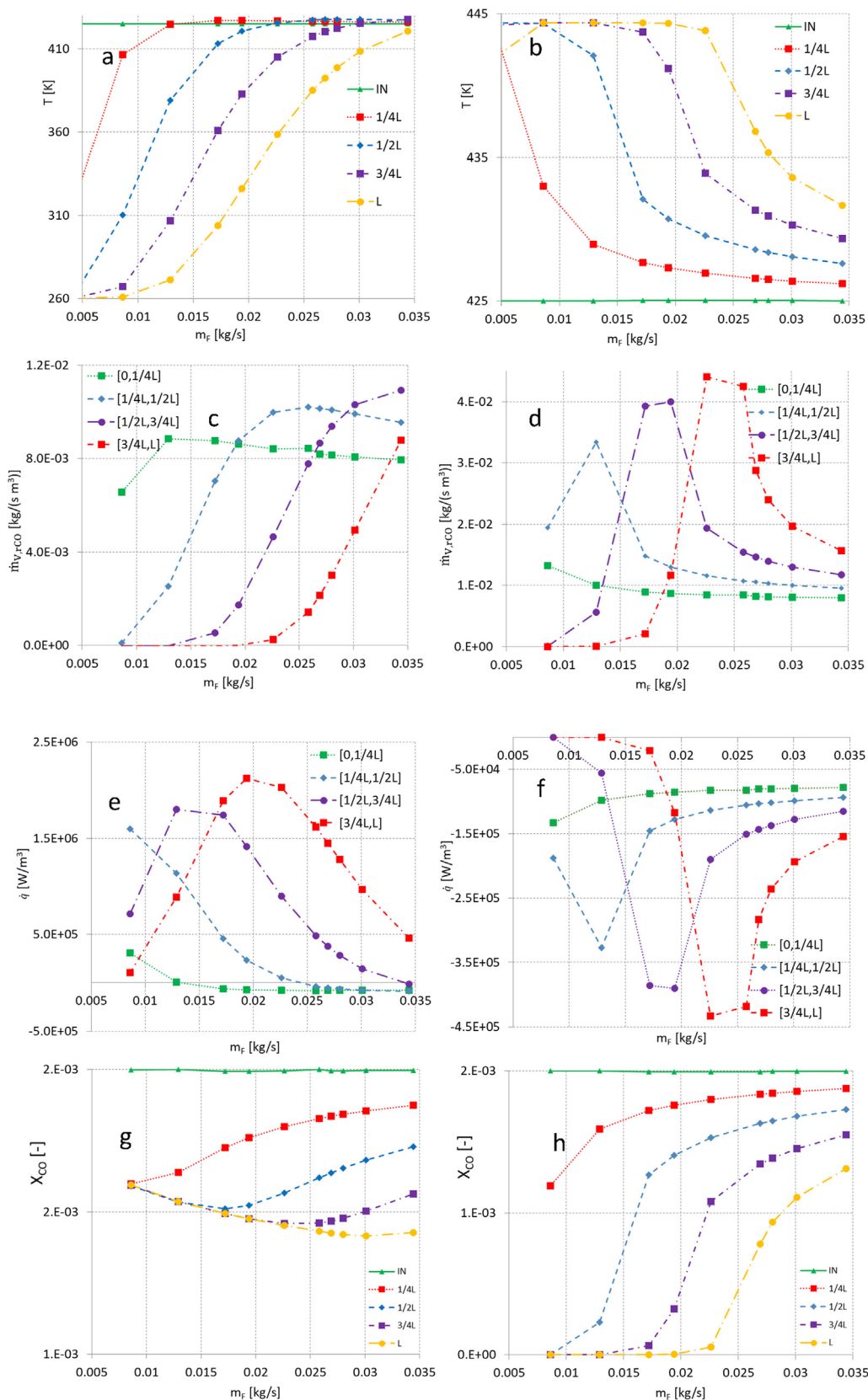


Fig. 13. Temperature, T_F , (a,b), reacting mass flux $\dot{m}_{V,CO}$ on the solid surface (c,d), convective heat flux, \dot{q} , per unit volume (e,f), CO concentrations, X_{CO} , (g,h), in function of \dot{m}_F in different locations (IN, 1/4L, 1/2L, 3/4L, L) inside AM1, at $t = 50$ s (a,c,e,g) and at $t = 400$ s (b,d,f,h) ($T_{SO} = 260$ K and $T_{Fin} = 425$ K).

The temperature in the position where CO conversion is completed, as well as in all further downstream positions, is only a function of the entering CO concentration, and is independent from \dot{m}_F . This is clear from Eq. (15), which describes the heat equilibrium:

$$\dot{m}_{r,CO}LHV = \dot{m}_F C_{pF} \Delta T \quad (15)$$

Given that

$$\dot{m}_{r,CO} = \dot{m}_F (X_{CO,F,in} - X_{CO,F,out}) \quad (16)$$

and that $X_{CO,F,out} = 0$ at the position where CO is fully converted, then:

$$\Delta T = T_F(x(X_{CO} = 0)) - T_{Fin} = \frac{LHV}{C_{pF}} X_{CO,F,in} \quad (17)$$

For $X_{CO,F,in} = 3000$ ppm used in this study, $\Delta T = 19$ K, and thus, $T_F(x > x(X_{CO} = 0)) = 444$ K.

In Fig. 13d the corresponding CO reacting mass flow $\dot{m}_{v,rCO}$ on the catalyst surface in each quarter is described in function of \dot{m}_F . At $t = 400$ s. Fig. 13d shows the space distribution of the reactions. For the lowest \dot{m}_F examined ($=0.0086$ kg/s), all CO reacts within the first two quarters. Consequently, the fluid has a maximum temperature of 444 K downstream the first half ($T(x = 1/2L) = T(x = 3/4L) = T(x = L) = 444$ K). For the next higher $\dot{m}_F = 0.012$ kg/s, reactions occur in the first three quarters of the converter. Precisely, the temperature at $x = 1/4L$ is lower, thus also the corresponding reaction rate is lower. In the second quarter, a similar decrease in temperature occurs, given the higher amount of gases to be heated up. However, $\dot{m}_{v,rCO}$ is higher in respect to the one at the lower \dot{m}_F . Moreover, reactions start happening in the third quarter. The maximum $T_F = 444$ K characterizes the converter at $x = 3/4L$ and at $x = L$. Analogously, at $\dot{m}_F = 0.0168$ kg/s, reactions occur along the entire converter. The equilibrium temperatures at $x = 1/4L$, $x = 1/2L$ and at $x = 3/4L$ decrease, as do $\dot{m}_{v,rCO}$ at $x = 1/4L$ and at $x = 1/2L$. Reactions in the third quarter are stronger, and start also in the last quarter. The maximum $T_F = 444$ K is now only reached at the end of the converter. For $\dot{m}_F > 0.0194$ kg/s the reaction rates in the entire catalytic converter are not high enough to oxidize the entire CO entering. In order to achieve full conversion, a longer catalytic converter would be needed. In fact, for $\dot{m}_F > 0.0194$ kg/s, reactions are stronger in the downstream catalyst parts. The heat released is lower and has to heat up a larger amount of fluid, thus the resulting temperature increase over T_{Fin} is lower at each position in respect to the temperatures at lower mass flows.

In contrast to $t = 50$ s, at $t = 400$ s, temperatures increase along the converter for each \dot{m}_F (Fig. 13b). For example, at $\dot{m}_F = 0.012$ kg/s, $T_F(x = L) > T_F(x = 3/4L) \dots > T_F(x = 1/2L)$. An additional important implication can be deduced by comparing Fig. 13a, b. At $t = 50$ s and as long as the catalytic converter is in the initial heat-up phase, increasing \dot{m}_F accelerates the heat up process. In contrast, in the second phase (slightly to be seen in $t = 50$ s and clearly at $t = 400$ s), increasing \dot{m}_F beyond a limit hinders the heat up leading to lower temperatures.

In Fig. 13f the heat transferred from the fluid to the solid is shown. At 400 s, \dot{q} , is primarily based on the heat released by the chemical reactions in the solid (which in turn is convected back to the fluid). This is the reason of the negative sign (heat convected from the solid to the fluid). The considerations related to Fig. 4 for $\dot{m}_F = 0.0172$ kg/s can be generalized for the entire \dot{m}_F range investigated. Moreover, comparing Fig. 13e,f, it is clear that the magnitude of \dot{q} at 400 s is approximately 10 times less with respect to the one at 50 s. The behavior of \dot{q} at 400 s in function of \dot{m}_F reflects the behavior already described in Fig. 13d for the $\dot{m}_{v,rCO}$.

The influence of varying \dot{m}_F on X_{CO} at $t = 400$ s is described in Fig. 13h. $X_{CO,in}$ is indicated in green. For the lowest $\dot{m}_F = 0.0086$ kg/s considered, all reactions occur in the first half of the catalytic converter, X_{CO} in all the further downstream sections is zero. For increasing \dot{m}_F , X_{CO} at the end of the first half increases and reactions start gradually in the following sections. Analogously, also X_{CO} at $x = 1/2L$, $x = 3/4L$ and L increase for increasing \dot{m}_F . For $\dot{m}_F < 0.0194$ kg/s the converter is able to reach full conversion (CO concentration at $x = L$ is zero). With $\dot{m}_F > 0.0194$ kg/s, the converter length is not enough for full CO conversion.

3.5. Similarity of the instationary heat transfer

Fig. 14 describes the dimensionless temperature response of AM1, θ_F , as a function of the dimensionless time-space coordinate τ/ξ . Different lines correspond to different conditions, i.e. out of $T_S(t = 0) = [260,360]$ K, $T_{Fin} = [410,425]$ K and $\dot{m}_F = [0.0086,0.0172]$ kg/s, and to different catalytic converter lengths ($1/2L$ and L). All lines have the characteristic S-shape. The initial $\theta(T_S = T_S(t = 0)) = T_0 = 0$ and approaches unity ($T_S = T_{Fin}$) at the end of the initial heat-up phase. Values higher than 1 correspond to the second phase of the warm up and are results of heat released by the reactions. Interestingly, the temperature rise for larger catalytic converter lengths occurs later, but it is steeper so that the asymptotic temperature is achieved earlier. Even \dot{m}_F influences θ_F response. The temperature rise for lower \dot{m}_F occurs later, but it is steeper so that the asymptotic temperature is achieved earlier. Important to notice is that $\theta_F = 0.56$ for τ/ξ close to 1. The values we found are very similar to those in (Koltzakis, 1997). The heat up of a converter can be approximated by an analytical expression using a double exponential function of the type:

$$\theta = \theta\left(\frac{\tau}{\xi}\right) = 1 - e^{-k\left(\frac{\tau}{\xi}\right)^m} \quad (18)$$

The k parameter is independent from ξ and can be found by substituting the point $(\tau/\xi) = (1, 0.56)$ in Eq. (18), $k = \ln(1 - 0.56) = -0.82$. Given the differences in the steepness of the lines in Fig. 14, the exponent m should be a function of ξ . The method of least-squares approximation has been employed to find the best correlation between m and ξ , the result is:

$$m = 1.7\xi^{-0.21} \quad (19)$$

The implications of Eq. (17) are of some interest for simplifying the numerical approach. First of all, it is clear that an equation similar to Eq. (17) can only describe the phenomena with some accuracy when the second term of Eq. (8), $\Lambda \frac{\partial^2 \theta_s}{\partial \xi^2}$, is small relatively to the third one, $\frac{\partial \theta_F}{\partial \xi}$ (and at negligible heat release due to chemical

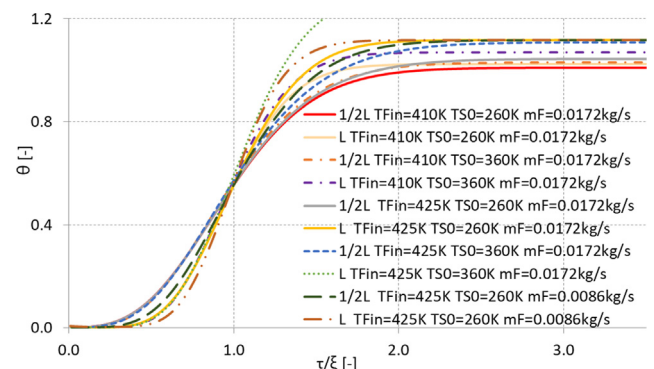


Fig. 14. θ_F in function of τ/ξ , with varying $T_S(t = 0) = [260,360]$ K, $T_{Fin} = [410,425]$ K, $\dot{m}_F = [0.0086,0.0172]$ kg/s and $x = [1/2L,L]$.

reactions). This is the case when Λ is small, thus small or negligible axial heat conduction in the solid. This is also the case for the catalytic converter in question (ceramic material) in the present work, (it is not the case when considering metallic catalyst substrates). In addition, Eq. (17) gives an analytical solution of the time and location dependent temperatures, should m and k be known. So, by knowing m and k (through either previous simulations or experiments), the analytical solution provided by Eq. (18) can simplify the computations and the numerical solution of Eq. (8).

3.6. Comparison between different AM geometries

The AM structure studied in the previous sections, called for simplicity AM1, has $\varepsilon = 0.8$, $d_s = 0.8$ mm and $S_V = 896$ m²/m³ (according to analytical approximation models in (Papetti et al., 2018)). It was chosen for been similar to the realized vehicle catalysts (see Section 2.1), having though thinner struts and only slightly improved properties. In this section, AM1 is compared with the two further AM structures (Table 2) in terms of temperature and CO conversion behavior during transient operating conditions. The three different geometries have been chosen for their different porosity ε , strut diameter d_s , and thus specific surface area S_V . Based on Table 2 and taking into consideration fixed converter outer dimensions (overall converter volume of 2lt), AM2 has the highest ε , thus the lowest converter mass. Moreover, AM3 has also slightly lower mass than AM1, given its higher porosity. Considering that the mass of each catalytic converter is a function of its porosity: $m_s = m_{AM} = (1 - \varepsilon)V \cdot \rho$, values from Table 2 give:

$$m_{AM2} < m_{AM3} < m_{AM1} \quad (20)$$

more specifically: $m_{AM3} = 0.75m_{AM1}$ and $m_{AM2} = 0.5m_{AM1}$.

It is also relevant to notice that AM3 has the highest S_V , thus the highest wetted surface S_W (at fixed overall converter volume of 2lt), while AM2 the lowest.

$$S_{VAM2} < S_{VAM1} < S_{VAM3} \quad (21)$$

Fig. 15 compares the time evolution of T_F (a) and X_{CO} (b) for the three different structures (similar to Fig. 4 for AM1). Displayed are the time histories only at the positions $x = 1/4L$ and $x = L$. The results correspond to the case of $T_{Fin} = 425$ K, $T_{S0} = 260$ K and $\dot{m}_F = 0.0172$ kg/s. On the whole, the warm up is similar among the different cases examined and the mechanism is the one already described in detail in Section 3.1. However, the heat up characteristics in terms of rates and durations differ among the AM structures. AM2 shows the fastest heat up and the steepest temperature increase. This is valid in the initial heat-up phase, when the catalytic converter is heated up by the fluid. AM2 is followed by AM3, while AM1 is the structure with the slowest heat-up characteristic. This behavior can be well explained with some

basic reasoning. During the initial heat-up phase, heat is transferred from the fluid to the solid. The heat transferred in a time step is proportional to

$$Q_{F \rightarrow S} \propto (h \cdot S_W \cdot \Delta T_F) \quad (22)$$

The heat transfer coefficient, h , is given by

$$h = \frac{Nu\lambda}{d_s} \quad (23)$$

Assuming that the heat and mass transfer analogy holds, then the Nusselt number's dependency on the strut diameter d_s must be similar to the Sherwood number's dependency on d_s according to (Papetti et al., 2018):

$$Nu = f(d_s^{0.3}) \quad \text{just as} \quad Sh = f(d_s^{0.3}) \quad (24)$$

Thus $h = f(d_s^{-0.7})$, so that $h_{AM3} = h_{AM2} = 1.39h_{AM1}$.

The surface, corresponding to S_W , on the other hand, is $S_{W,AM3} = 1.43S_{W,AM2}$ and $S_{W,AM1} = 1.22S_{W,AM2}$ based on the values reported in Table 2. This gives a rough estimation of the ratio of the heat transferred from the fluid to the solid among the three structures during one time step:

$$Q_{F \rightarrow S,AM3} = 1.43Q_{F \rightarrow S,AM2} \quad (25)$$

$$\text{and} \quad Q_{F \rightarrow S,AM2} = 1.14Q_{F \rightarrow S,AM1} \quad (26)$$

So the heat transferred from the fluid to the solid in one time step, assuming similar temperature gradients (for the beginning of the heat-up process at least is an acceptable assumption) is highest for AM3, followed by AM2 and then AM1. This amount of heat increases the internal energy of the solid (when neglecting the anyhow low conduction in the solid):

$$Q_{F \rightarrow S} = m_s c_p \left(\frac{dT_s}{dt} \right)_{AM} \quad (27)$$

Considering: $m_{AM3} = 1.5m_{AM2}$ and $m_{AM1} = 2m_{AM2}$ this simplified estimation yields:

$$\left(\frac{dT}{dt} \right)_{AM2} = 1.05 \left(\frac{dT_s}{dt} \right)_{AM3} \quad (28)$$

and

$$\left(\frac{dT}{dt} \right)_{AM2} = 1.75 \left(\frac{dT_s}{dt} \right)_{AM1} \quad (29)$$

The characteristics in Fig. 15 reflect quite well the approximations in Eqs. (28) and (29) since AM2 heats up first, followed by AM3 and then by AM1 (substantially later). Thus, on the surface of AM2, the initial chemical reactions and the 2nd heat-up phase, initiate earlier. Later in time the three structures end-up with identical temperature of 444 K. This is clear, given that with all three structures full CO oxidation is reached (according to the reasoning

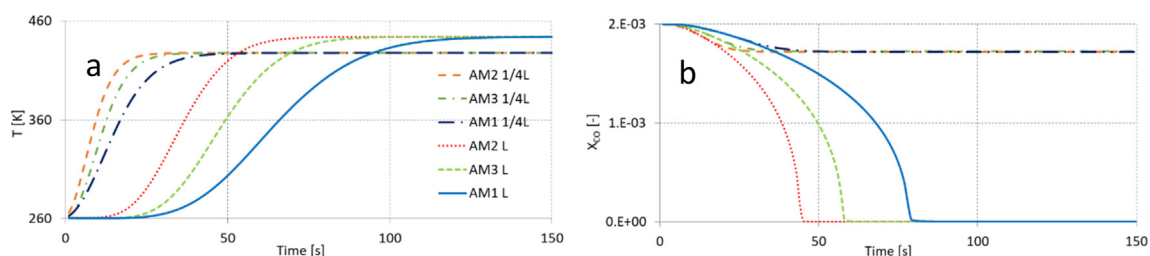


Fig. 15. Comparison of the three different AM structures (see Table 2) in terms of T_F (a) and X_{CO} (b) time histories in different locations (1/4L, L) ($T_{Fin} = 425$ K, $T_{S0} = 260$ K and $\dot{m}_F = 0.0172$ kg/s).

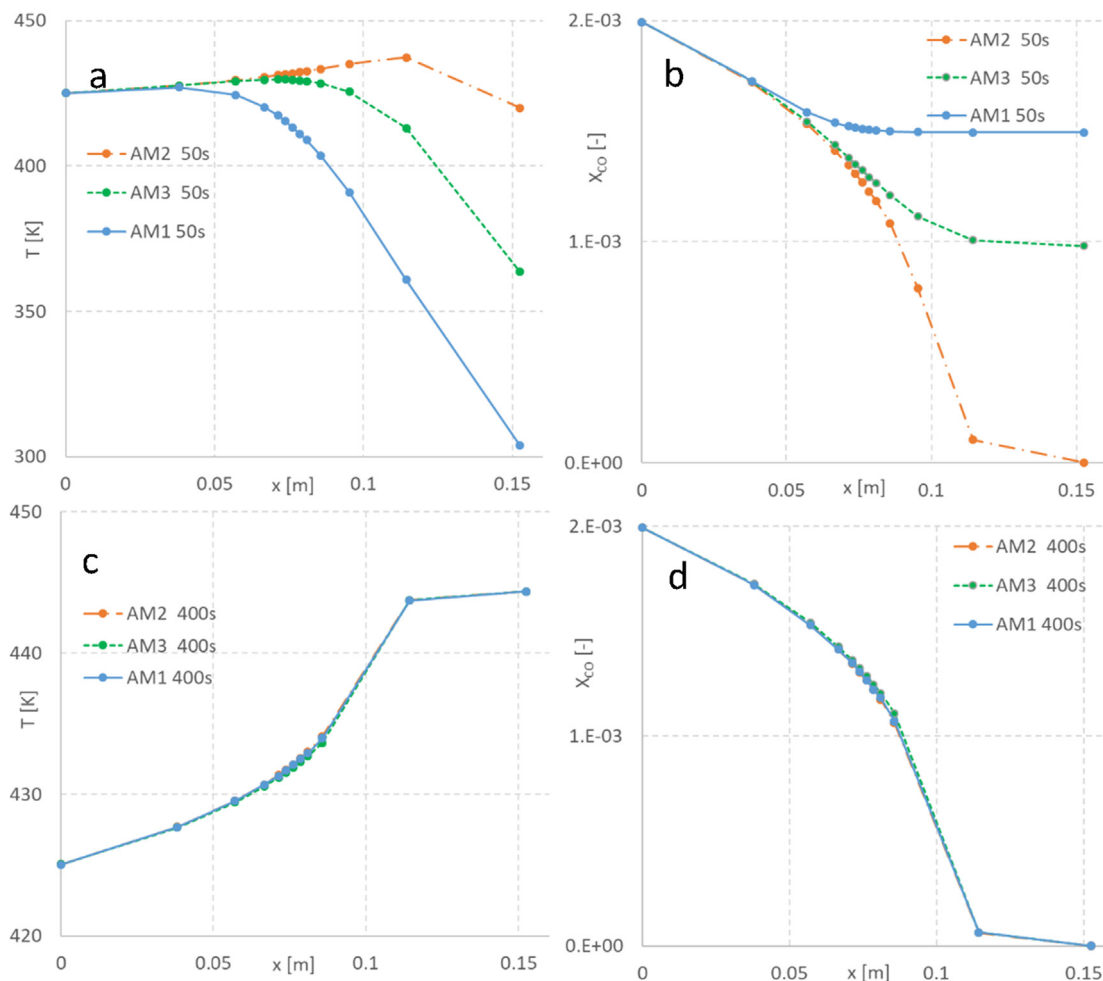


Fig. 16. Comparison of three different AM structures (see Table 2) in terms of spatial distribution of the T_F and the X_{CO} at the instants $t = 50$ s (respectively a and b) and $t = 400$ s (respectively c and d) along the converter length ($T_{Fin} = 425$ K, $T_{S0} = 260$ K and $\dot{m}_F = 0.0172$ kg/s).

of Eq. (17)). Fig. 15b shows the corresponding X_{CO} time history at the same space positions $x = 1/4L$ and $x = L$ along the catalytic converter for the three different AM structures. The same case of $T_{S0} = 260$ K, $T_{Fin} = 425$ K and $\dot{m}_F = 0.0172$ kg/s is considered. The behavior described in Fig. 4 is similar for all the three different AM structures and directly depends on the temperature evolution. AM2 is thus the first to start reactions and to reach steady state at $x = 1/4L$ as well as at $x = L$, while AM1 is instead the slowest.

In Fig. 16, the three different AM structures are compared in terms of spatial distributions along the converter length (space coordinate x) of T_F (a,c) and X_{CO} (b,d) for the time instant $t = 50$ s (respectively a and b) and $t = 400$ s (respectively c and d). These two different time instants are already considered in Fig. 13: 50 s is typical for the initial warm-up phase, while $t = 400$ s shows the stationary phase, where equilibrium between the heat released at the solid surface is balanced by the heat transfer to the fluid. In Fig. 16a the three AM structures show a distinctive behavior. At $t = 50$ s the first part of the converter ($x < 0.05$ m) has reached and exceeded T_{Fin} for all three examined structures. This is consistent with the temperature time histories in Fig. 15a for the first catalyst quarter ($x = 1/4L$). Further downstream, the temperature differences among the three structures increase. AM2 has reached highest temperatures at these 50 s and is in the second heat-up phase almost along the entire catalytic converter (except the last downstream part). Chemical reactions and thus CO concentration reduction occur over the entire catalytic converter and almost full conversion is reached at full length. AM3 reaches similar tempera-

tures as AM2 for $x < 0.08$ m. For $x > 0.08$ m, however, the fluid has not been heated enough to induce full conversion, the reactions are weaker and the CO concentration higher. Finally, in the very last part of the AM3 catalyst, T_F is so low (at $t = 50$ s) that the reactions are negligible and X_{CO} remains almost constant. T_F in AM1 are generally lower and X_{CO} higher. In fact, at $t = 50$ s, for AM1 the fluid has recovered T_{Fin} in the upstream converter part, while it is cooled by the cooler solid in the remaining part. This T_F corresponds in Fig. 16b to a X_{CO} that is decreasing in the first part of the converter, as the result of weak chemical reactions, and is remaining constant in the downstream catalyst part.

The comparison is different when considering $t = 400$ s: all the three AM structures are in the second phase of the warm up and T_F increases along the converter length. Moreover, all the three AM structures behave almost identically, although they have significantly different S_W . This is evidence that in the relatively low temperature domain under investigation, the slow chemical reactions are the limiting mechanism. In addition, Fig. 16 confirms that a significant part of the reactions occurs in the downstream part of the catalytic converter, roughly the half of the entering CO is oxidized in the last third of the catalytic converter. These considerations reported for $\dot{m}_F = 0.0172$ kg/s are also valid for the entire \dot{m}_F range examined, as it can be noticed in Fig. 17. Whereas for $\dot{m}_F < 0.02$ kg/s the full conversion is reached, for $\dot{m}_F > 0.02$ kg/s the catalyst length is not sufficient therefore. With increasing \dot{m}_F , T_F at the catalytic converter exit decreases while the X_{CO} increases. As already described for AM1 in Fig. 13b, the main driver is the heat

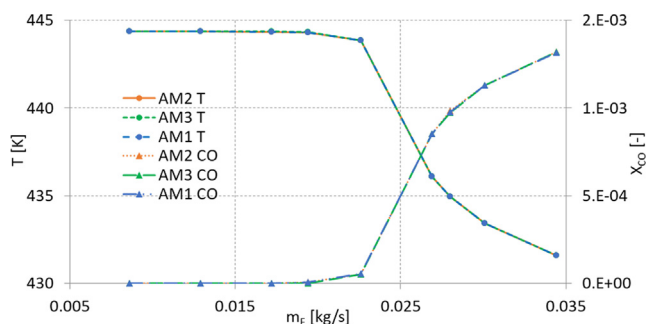


Fig. 17. Comparison of the three different AM structures (see Table 2) in terms of T_F and X_{CO} (a) at time instant 400 s in function of \dot{m}_F at the converter exit ($T_{Fin} = 425$ K, $T_{S0} = 260$ K).

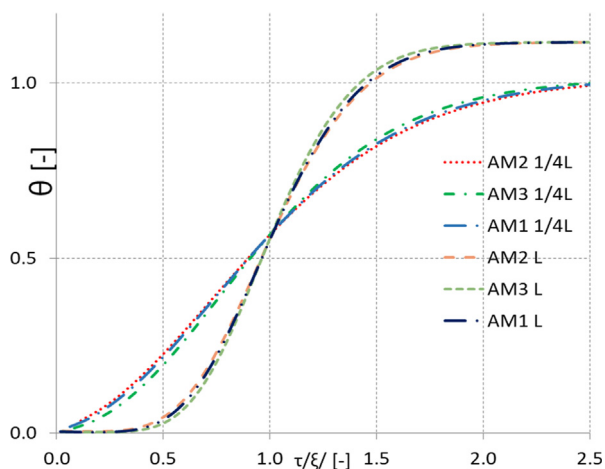


Fig. 18. θ_F in function of τ/ξ , for the different AM structures (see Table 2). Two different positions are considered ($x = 1/4L$ and $x = L$) ($T_{S0} = 260$ K, $T_{Fin} = 425$ K, $\dot{m}_F = 0.0172$ kg/s).

released by the chemical reactions on the solid surface and its convection to the fluid. All the AM structures considered are able to reach the same T_F and X_{CO} for all the \dot{m}_F considered. This also means that all the AM structures have sufficient surface and heat transfer properties for reaching the same final steady state.

Fig. 18 compares the three different AM structures (see Table 2) in terms of θ_F as a function of τ/ξ . Different lines correspond to the same fluid conditions ($T_{S0} = 260$ K, $T_{Fin} = 425$ K and $\dot{m}_F = 0.0172$ kg/s), but to two different catalytic converter lengths, $x = [1/4L, L]$. The characteristic S-type shape of Fig. 14 is clearly recognized here for all the cases. The double exponential function in Eq. (17) is still valid and, independently of the value of ξ , the characteristic time-space needed for the fluid temperature to reach almost half the way to its final value corresponds to 1. Thus the analytical approach, as described by Eq. (17) and (18), is also valid and can be used for catalysts with different lattice geometrical characteristics.

4. Conclusions

Automotive catalytic reactors should be carefully designed to minimize their thermal response times, in order to reach their nominal operating temperature as fast as possible and to minimize cold start emissions. In this study, the heat up of Additive Manufactured (AM) open cell polyhedral catalytic substrates during cold start has been analyzed using experiments on chassis dynamometer, numerical simulation and analytical methods. The typical

automotive catalytic converter cold start is characterized by gases from the engine at moderate temperatures arriving in the entrance of the converter, which has a lower, often ambient, temperature. In order to study the fundamental mechanisms involved, the cases investigated have been setup with exhaust gas of constant, moderate temperatures and mass flow rates flowing in an adiabatic catalytic converter with an initial, lower, uniform temperature. The focus was set on the temporal and spatial profiles of the temperature and CO concentration inside and at the exit of the converter. All simulations have been performed in OpenFOAM.

In all examined cases, two different phases during the heat-up have been distinguished:

- In the initial phase, the gases warm-up the solid-converter, $T_S < T_F < T_{Fin}$, (convection from fluid to solid aided by initial oxidation reactions) until $T_S = T_F = T_{Fin}$. The gases warm-up the solid-converter through convection. The heat up is helped by initial oxidation reactions in the upstream converter part.
- The second phase starts when the converter and the fluid inside have reached the same temperature, equal to the one of the fluid entering the converter. This phase is characterized by the heat released by the reactions, thus the heat transfer is from the solid to the fluid and $T_S > T_F > T_{Fin}$.

In the first instants of the initial phase, the gases warm-up the solid catalytic converter in the entrance region and are cooled down towards the initial solid temperature in the downstream. Main characteristics of this phase are:

- The duration of the first phase is different along the converter and downstream locations experience a longer first phase. However, the duration is independent from the initial temperature difference between solid and fluid.
- The heat transferred (in energetic terms) is relatively homogeneously distributed throughout the catalytic converter and, in any location, it increases in time towards a peak and decreases thereafter. The heat transfer peak is highest in upstream locations and decreases in the downstream. The heat exchanged is strongly dependent from the initial temperature difference between solid and fluid.
- At each instant, temperatures decrease along the converter length.
- Increasing \dot{m}_F accelerates the initial heat up, resulting in higher temperatures at fixed time instants at all locations.
- The introduction of dimensionless temperature differences, dimensionless time and dimensionless space coordinates evidences the similarity of all examined cases (i.e. for different mass flow rates, flow inlet and catalytic converter initial temperatures as well as lengths).
- The catalytic converter heat up, expressed with the dimensionless parameters, has the characteristic S-type shape, and is a double logarithmic function that can be approximated by a corresponding analytical expression. A larger converter heats up slower at first but then at an accelerated rate.
- Under the hypothesis of negligible solid conductivity, the characteristic dimensionless time-space τ/ξ needed for the outlet solid temperature to reach almost half the way to its final value corresponds to 1.

The second phase is characterized by:

- The driving phenomena are chemical reactions. As upstream locations are warmed-up first, the onset of chemical reactions first occurs upstream. The heat released by the reactions is transported downstream resulting in a faster increase of tem-

peratures and reaction rates (as long as enough reactants are there). Stationary conditions are reached almost instantly, leading to constant local temperatures and reaction rates in time.

- The enthalpy of the inflowing gases has to be matched to the energy released by the chemical reactions, for achieving the fastest possible warm up. If the mass flow is too high, only a modest and slow temperature increase can be achieved. On the other hand, if full conversion is achieved, the highest temperature is reached at the location where the last remaining CO is oxidized. This temperature is a function only of the inflowing CO concentration and is independent of the fluid mass flow.
- Temperatures are generally higher in the downstream than in the upstream converter part. This leads to higher reaction rates and thus to higher reaction heats released in the downstream locations.
- The initial solid temperature influences the onset of this second phase, while the inlet fluid temperature and the inlet CO concentration influences the local equilibrium temperature.
- Increasing fluid mass flow results in lower local temperature increase in respect to the temperature of the inflowing gases.

Three AM converter substrates with different geometrical properties, thus different thermal and mechanical properties and different mass, have been compared in terms of thermal and conversion characteristics:

- Lighter structures (higher ε) allow a faster initiation of the warm up, have shorter first phase duration and require less heat exchanged for reaching a target temperature
- Structures characterized by higher Nu levels show a faster warm up, have shorter first phase duration and require less heat exchanged for reaching a target temperature
- During the second phase of the warm up process, after reaching stationarity, when the main phenomena are the chemical reactions and the consequent heat released from the solid surface to the fluid, the AM behavior is almost independent from thermal, mass and surface properties
- The dimensionless as well as the analytical approach proposed for the initial heat-up phase is valid also for catalysts with different geometrical lattice parameters.

CRedit authorship contribution statement

All the authors have contributed to the Conceptualization, Data Curation, Formal Analysis, Investigation, Methodology and Writing-review and editing of the entire paper.

Declaration of Competing Interest

The authors declare that they have no known competing financial interests or personal relationships that could have appeared to influence the work reported in this paper.

Acknowledgements

The authors gratefully acknowledge the Swiss federal Office for Environment for the project “Modellierung und Validierung des Katalysatorverhaltens bei Kaltstart und im Gesamtzyklus”, contract no 15.0002.PJ / S122-1359 and the project “Development and manufacturing of an automotive catalyst concept for cold start low exhaust temperatures”, Project No UTF 511.14.15 IDM2006.2423.485 for the financial support.

The authors gratefully acknowledge also financial support from the Swiss National Science Foundation (SNF) for the project “Cases: Catalyst Substrates from Engineered Structures for state of the art

powertrains: High pollutant conversion (including cold-start) with low precious metal requirements”, Project No 20PC21_161571/1.

References

- Bianchi, E., Heidig, T., Visconti, C.G., Groppi, G., Freund, H., Tronconi, E., 2012. An appraisal of the heat transfer properties of metallic open-cell foams for strongly exo-/endo-thermic catalytic processes in tubular reactors. *Chem. Eng. J.* 198–199 (August), 512–528.
- Bianchi, E., Heidig, T., Visconti, C.G., Groppi, G., Freund, H., Tronconi, E., 2013. Heat transfer properties of metal foam supports for structured catalysts: wall heat transfer coefficient. *Catal. Today* 216 (November), 121–134.
- Braconi, M., Ambrosetti, M., Maestri, M., Groppi, G., Tronconi, E., 2018. A fundamental investigation of gas/solid mass transfer in open-cell foams using a combined experimental and CFD approach. *Chem. Eng. J.* 352, 558–571. <https://doi.org/10.1016/j.cej.2018.07.023>.
- Busse, C., Freund, H., Schwieger, W., 2018. Intensification of heat transfer in catalytic reactors by additively manufactured periodic open cellular structures (POCS). *Chem. Eng. Process. Process Intensif.* 124, 199–214.
- Chen, D.K.S., Bissett, E.J., Oh, S.H., Van Ostrom, D.L., 1988. A three dimensional model for the analysis of transient thermal and conversion characteristics of monolithic catalytic converters. *SAE Technical Paper* 880282, doi:10.4271/880282.
- Della Torre, A., Montenegro, G., Onorati, A., Cerri, T., 2018. CFD Investigation of the impact of electrical heating on the light-off of a diesel oxidation catalyst. *SAE Technical Paper* 2018-01-0961, doi:10.4271/2018-01-0961.
- Della Torre, A., Montenegro, G., Onorati, A., Cerri, T., 2018. CFD investigation of the impact of electrical heating on the light-off of a diesel oxidation catalyst. *SAE Technical Paper* 2018-01-0961, doi:10.4271/2018-01-0961.
- Della Torre, A., Montenegro, G., Onorati, A., Tabor, G., 2015. CFD characterization of pressure drop and heat transfer inside porous substrates. *Energy Procedia*. 81, 836–845. <https://doi.org/10.1016/j.egypro.2015.12.093>.
- Depcik, C., Assanis, D., 2005. One-dimensional automotive catalyst modeling. *Prog. Energy Combust. Sci.* 31, 308–369.
- Dimopoulos Eggenschwiler, P., Tsinoglou, D.N., Seyfert, J., Bach, C., Vogt, U., Gorbar, M., 2009. Ceramic foam substrates for automotive catalyst applications: Fluid mechanic analysis. *Exp. Fluids*. 47, 209–222. <https://doi.org/10.1007/s00348-009-0653-2>.
- Dimopoulos Eggenschwiler, P., Papetti, V., Lucci, F., Ortona, A., 2018. Additive manufactured open cell structures: Promising substrates for automotive catalysts. In: *Proceedings of the 18th Stuttgart International Symposium, Automotive and Engine Technology*. https://doi.org/10.1007/978-3-658-21194-3_24.
- Gaiser, G., Oesterle, J., Braun, J., Zacke, P., 2003. The progressive spin inlet - homogeneous flow distributions under stringent conditions. *SAE Technical Paper* (2003-01-0840), doi:10.4271/2003-01-0840.
- Giani, L., Groppi, G., Tronconi, E., 2005. Mass-transfer characterization of metallic foams as supports for structured catalysts. *Ind. Eng. Chem. Res.* 44, 4993–5002. <https://doi.org/10.1021/ie0490886>.
- Giani, L., Groppi, G., Tronconi, E., 2005. Heat transfer characterization of metallic foams. *Ind. Eng. Chem. Res.* 44, 9078–9085.
- Gräf, I., Rühl, A.-K., Kraushaar-Czarnetzki, B., 2014. Experimental study of heat transport in catalytic sponge packings b y monitoring spatial temperature profiles in acocooled-wallreactor. *Chem. Eng. J.* 244 (May), 234–242.
- Hayes, R.E., Kolaczkowski, S.T., 1994. Mass and heat transfer effects in catalytic monolith reactors. *Chem. Eng. Sci.* 49 (21), 3587–3599.
- Heck, R.H., Wei, J., Katzer, J.R., 1976. Mathematical modeling of monolithic catalysts. *AIChE J.* 22 (3), 477–484.
- Kays, W.M., Crawford, M.E., 1993. *Convective Heat and Mass Transfer*. McGraw-Hill, New York, U.S.A.
- Koltsakis, G., 1997. Warm-up behavior of monolithic reactors under non-reacting conditions. *Chem. Eng. Sci.* 53, 2891–2899.
- Koltsakis, G.C., Katsaounis, D.K., Samaras, Z.C., Naumann, D., Saberi, S., Böhm, A., Markomanolakis, I., 2008. Development of metal foam based aftertreatment system on a diesel passenger car, doi:10.4271/2008-01-0619.
- Koltsakis, G.C., Konstantinidis, P.A., Stamatelos, A.M., 1997. Development and application range of mathematical models for 3-way catalytic converters. *Appl. Catal. B* 12, 161–191.
- Kopanidis, A., Theodorakakos, A., Gavaises, E., Bouris, D., 2010. 3D numerical simulation of flow and conjugate heat transfer through a pore scale model of high porosity open cell metal-foam. *Int. J. Heat Mass Transf.* 53, 2539–2550.
- Krishnan, S., Murthy, J.Y., Garimella, S.V., 2006. Direct simulation of transport in open-cell metal-foam. *J. Heat Transf.* 128, 793.
- Lin, T.F., Kuo, J.C., 1988. Transient conjugated heat transfer in fully developed laminar pipe flows. *Int. J. Heat Mass Transfer* 31 (5), 1093–1102.
- Lu, T.J., Stone, H.A., Ashby, M.F., 1998. Heat transfer in open-cell metal foams. *Acta Mater.* 46, 3619–3635. [https://doi.org/10.1016/S1359-6454\(98\)00031-7](https://doi.org/10.1016/S1359-6454(98)00031-7).
- Lucci, F., Della Torre, A., von Rickenbach, J., Montenegro, G., Poulikakos, D., Dimopoulos Eggenschwiler, P., 2014. Performance of randomized Kelvin cell structures as catalytic substrates: mass-transfer based analysis. *Chem. Eng. Sci.* 112, 143–151. <https://doi.org/10.1016/j.ces.2014.03.023>.
- Lucci, F., Della Torre, A., Montenegro, G., Kaufmann, R., Dimopoulos Eggenschwiler, P., 2017. Comparison of geometrical, momentum and mass transfer characteristics of real foams to Kelvin cell lattices for catalyst applications.

- Int. J. Heat Mass Transf. 108, 341–350. <https://doi.org/10.1016/j.jheatmasstransfer.2016.11.073>.
- Oh, S.H., Cavendish, J.C., Hegedus, L.L., 1980. *AIChE J.* 26, 935.
- Oh, S.H., Cavendish, J.C., 1985. *AIChE J.* 31 (6), 943–947.
- Oh, S.H., Cavendish, J.C., 1985. *AIChE J.* 31 (6), 935–942.
- Olek, S., Elias, E., Wacholder, E., Kaizerman, S., 1991. Unsteady conjugated heat transfer in laminar pipe flow. *Int. J. Heat Mass Transfer* 34 (6), 1443–1450.
- Pangarkar, K., Schildhauer, T.J., Van Ommen, J.R., Nijenhuis, J., Kapteijn, F., Moulijn, J. A., 2008. Structured packings for multiphase catalytic reactors. *Ind. Eng. Chem. Res.* 47 (10), 3720–3751. <https://doi.org/10.1021/ie800067r>.
- Papetti, V., Dimopoulos Eggenschwiler, P., 2019. Reduction of Cold Start emissions with Microwave heated Catalytic converters. In: Proceedings of the 19th Stuttgart International Symposium, Automotive and Engine Technology. https://doi.org/10.1007/978-3-658-25939-6_51.
- Papetti, V., Dimopoulos Eggenschwiler, P., Della Torre, A., Lucci, F., Ortona, A., Montenegro, G., 2018. Additive Manufactured open cell polyhedral structures as substrates for automotive catalysts. *Int. J. Heat Mass Transf.* 126, 1035–1047. <https://doi.org/10.1016/j.jheatmasstransfer.2018.06.61>.
- Papetti, V., Dimopoulos Eggenschwiler, P., Della Torre, A., Montenegro, G., Onorati, A., Koltsakis, G., 2019. Heat transfer analysis of catalytic converters during cold starts. SAE (Society of Automotive Engineers) Paper, 2019-24-0163, <https://doi.org/10.4271/2019-24-0163>.
- Santoliquido, O., Bianchi, G., Dimopoulos Eggenschwiler, P., Ortona, A., 2017. Additive manufacturing of periodic ceramic substrates for automotive catalyst supports. *Int. J. Appl. Ceram. Technol.* 14, 1164–1173. <https://doi.org/10.1111/ijac.12745>.
- Tsinoglou, D.N., Dimopoulos Eggenschwiler, P., Thurnheer, T., Hofer, P., 2009. A simplified model for natural gas vehicle catalysts with honeycomb and foam substrates. *Proc. Inst. Mech. Eng. Part D: J. Automob. Eng.* 223 (Jun. 6), 819–834.
- von Rickenbach, J., Lucci, F., Dimopoulos Eggenschwiler, P., Poulidakos, D., 2015. Pore scale modeling of cold-start emissions in foam based catalytic reactors. *Chem. Eng. Sci.* 138, 446–456. <https://doi.org/10.1016/j.ces.2015.08.020>.
- von Rickenbach, J., Lucci, F., Narayanan, C., Dimopoulos Eggenschwiler, P., Poulidakos, D., 2015. Effect of washcoat diffusion resistance in honeycomb and foam based catalytic reactors. *Chem. Eng. J.* 276, 388–397. <https://doi.org/10.1016/j.cej.2015.03.132>.
- Votruba, J., Sinkule, J., Hlavacek, V., Skrivanek, J., 1975. Heat and mass transfer in monolithic honeycomb catalysts-I. *Chem. Eng. Sci.* 30, 117–123.
- Yan, W.M., Tsay, Y.L., Lin, T.F., 1989. Transient conjugated heat transfer in laminar pipe flows. *Int. J. Heat Mass Transfer* 32 (4), 775–777.
- Young, L.C., Finlayson, B.A., 1974. Mathematical modeling of the monolith converter. *Adv. Chem. Ser.* 133, 629–643.
- Zygourakis, K., 1989. Transient operation of monolith catalytic converters: a twodimensional reactor model and the effects of radially nonuniform flow distributions. *Chem. Eng. Sci.* 44, 2075–2086. [https://doi.org/10.1016/0009-2509\(89\)85143-7](https://doi.org/10.1016/0009-2509(89)85143-7).